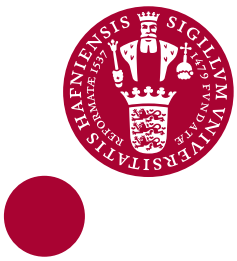

# Combining a Quantum Cascade Laser Spectrometer with an Automated Closed-Chamber System for delta 13 Measurements of Forest Soil, Tree Stem and Tree Root CO2 Fluxes

Brændholt, Andreas; Ibrom, Andreas; Ambus, Per; Larsen, Klaus Steenberg; Pilegaard, Kim

*Published in:*
Forests

*DOI:*
10.3390/f10050432

*Publication date:*
2019

*Document version*
Publisher's PDF, also known as Version of record

forests

MDPI

Article

# Combining a Quantum Cascade Laser Spectrometer with an Automated Closed-Chamber System for $\delta^{13}C$ Measurements of Forest Soil, Tree Stem and Tree Root $CO_2$ Fluxes

**Andreas Brændholt [1,2,*], Andreas Ibrom [1], Per Ambus [3], Klaus Steenberg Larsen [1,3] and Kim Pilegaard [1]**

1 DTU Environment, Technical University of Denmark, 2800 Kgs. Lyngby, Denmark; anib@env.dtu.dk (A.I.); ksl@ign.ku.dk (K.S.L.); kipi@env.dtu.dk (K.P.)
2 Department of Ecology and Evolutionary Biology, University of Arizona, Tucson, AZ 85719, USA
3 Department of Geosciences and Natural Resource Management, University of Copenhagen, 1958 Frederiksberg C, Denmark; peam@ign.ku.dk
* Correspondence: braendholt@email.arizona.edu

Received: 16 April 2019; Accepted: 17 May 2019; Published: 19 May 2019


**Abstract:** Recent advances in laser spectroscopy have allowed for real-time measurements of the $^{13}C/^{12}C$ isotopic ratio in $CO_2$, thereby providing new ways to investigate carbon cycling in natural ecosystems. In this study, we combined an Aerodyne quantum cascade laser spectrometer for $CO_2$ isotopes with a LI-COR LI-8100A/8150 automated chamber system to measure the $\delta^{13}C$ of $CO_2$ during automated closed-chamber measurements. The isotopic composition of the $CO_2$ flux was determined for each chamber measurement by applying the Keeling plot method. We found that the $\delta^{13}C$ measured by the laser spectrometer was influenced by water vapour and $CO_2$ concentration of the sample air and we developed a method to correct for these effects to yield accurate measurements of $\delta^{13}C$. Overall, correcting for the $CO_2$ concentration increased the $\delta^{13}C$ determined from the Keeling plots by 3.4‰ compared to 2.1‰ for the water vapour correction. We used the combined system to measure $\delta^{13}C$ of the $CO_2$ fluxes automatically every two hours from intact soil, trenched soil, tree stems and coarse roots during a two-month campaign in a Danish beech forest. The mean $\delta^{13}C$ was $-29.8 \pm 0.32$‰ for the intact soil plots, which was similar to the mean $\delta^{13}C$ of $-29.8 \pm 1.2$‰ for the trenched soil plots. The lowest $\delta^{13}C$ was found for the root plots with a mean of $-32.6 \pm 0.78$‰. The mean $\delta^{13}C$ of the stems was $-30.2 \pm 0.74$‰, similar to the mean $\delta^{13}C$ of the soil plots. In conclusion, the study showed the potential of using a quantum cascade laser spectrometer to measure $\delta^{13}C$ of $CO_2$ during automated closed-chamber measurements, thereby allowing for measurements of isotopic ecosystem $CO_2$ fluxes at a high temporal resolution. It also highlighted the importance of proper correction for cross-sensitivity with water vapour and $CO_2$ concentration of the sample air to get accurate measurements of $\delta^{13}C$.

**Keywords:** $\delta^{13}C$ of forest $CO_2$ fluxes; forest carbon cycling; stable isotopes; isotope laser spectroscopy; automated closed-chambers

## 1. Introduction

The isotopic composition of carbon in $CO_2$ of ecosystem fluxes can reveal quantitative information about both physiological processes and carbon cycling [1]. In forests, $CO_2$ enters the ecosystem via C3 photosynthesis, a process that favours the light isotope $^{12}C$ over the heavy isotope $^{13}C$ in $CO_2$ [2]. This results in a lower ratio of $^{13}C$ to $^{12}C$, often expressed by the $\delta$ notation as $\delta^{13}C$, of ecosystem C than in the

atmosphere [3]. The ecosystem ultimately loses C by respiration, where soil respiration ($R_{soil}$) accounts for more than half of forest ecosystem respiration [4]. $R_{soil}$ is traditionally measured as soil $CO_2$ flux by the closed chamber method, where a chamber is placed on top the soil and the flux is calculated based on the $CO_2$ concentration increase in the chamber headspace over time [5]. The increase in chamber $CO_2$ concentration can be measured with online laser-based spectroscopy and automated chamber systems have been constructed that provide measurements of soil $CO_2$ fluxes at a high temporal resolution [6–9]. Closed chambers have also been used to yield information about the $\delta^{13}C$ of $R_{soil}$. This requires measuring the change in $\delta^{13}C$ in the chamber headspace as the $CO_2$ concentration increases. By fitting a linear equation to the $\delta^{13}C$ and the reciprocal $CO_2$ concentration, a so-called Keeling plot, the source $\delta^{13}C$ of the respired $CO_2$ can be calculated [10]. In contrast to the measurements of $CO_2$ concentration, measurements of $\delta^{13}C$ have traditionally been done by labour-intensive manual field samplings followed by laboratory analysis by isotope-ratio mass spectrometers (IRMS) that provide high precision measurements of $\delta^{13}C$ but are bulky, unfit for field operation and most often only allow for measurements of discrete samples [11]. A recent, novel alternative to IRMS is the emerging use of laser spectroscopy capable of real-time, fast response measurements of $\delta^{13}C$. Laser spectrometers have the advantage of being able to perform high frequency, $\delta^{13}C$ measurements of a continuous air sample and to be operated under field conditions, similar to infrared gas analysers for $CO_2$. A few technologies have been developed in recent years for measuring $\delta^{13}C$ in ecosystems including wavelength-scanned cavity ring-down spectroscopy, tunable diode laser absorption spectroscopy and quantum cascade laser absorption spectroscopy [12–16]. Quantum cascade lasers can operate in the mid-infrared where $CO_2$ show strong fundamental vibrational bands, thus allowing for high precision measurements [17]. They have successfully been used to measure the isotopic flux of $CO_2$ at ecosystem scale by eddy covariance [18,19], for tree branch photosynthesis in the field [20] and for field measurement of $\delta^{13}C$ of $R_{soil}$ by closed chambers [21]. Although a high accuracy can be achieved, the instruments are found to be highly temperature sensitive, why they need to be placed in a temperature-controlled environment during field application, such as inside a temperature-controlled cabin or box [15,22]. Furthermore, closed path laser spectroscopy has been found to be influenced by changes in water vapour in the sample air, which dilutes the gas of interest and causes pressure line broadening that might act differently on $^{12}C$ and $^{13}C$, thus affecting the apparent measured $\delta^{13}C$ [23]. Likewise, concentration dependence might be present, which can cause the measured $\delta^{13}C$ to be influenced by the absolute concentration of $CO_2$ in a gas sample [24]. Both the influence of water vapour and the absolute $CO_2$ concentration dependence are instrument specific and must be determined for each individual instrument. For many purposes, including eddy covariance, the sample air can be dried, which eliminates the effect of water vapour on the measured $\delta^{13}C$ [19]. Furthermore, the change in $CO_2$ concentration over time during eddy covariance measurements is relatively small and thus, the concentration dependence may be limited. However, it still needs to be quantified, which has been done by varying the $CO_2$ concentration in calibration gases while keeping the $\delta^{13}C$ constant [25,26]. In contrast to eddy covariance, the concentration of both $CO_2$ and $H_2O$, as well as $\delta^{13}C$ may all change significantly during a closed-chamber measurement. In addition, sample air is constantly cycled in a loop between the chamber and the laser spectrometer, which can complicate or make it impossible to dry the air before it enters the laser, without potentially disturbing the chamber headspace environment. Thus, the effect of water vapour on $\delta^{13}C$ must be quantified. Furthermore, because the $\delta^{13}C$ of the flux is calculated based on the change in $CO_2$ concentration and $\delta^{13}C$ during a measurement, the concentration dependence of $\delta^{13}C$ in the range of $CO_2$ concentrations during a measurement must also be correctly quantified to accurately estimate $\delta^{13}C$.

In the current study we aimed to (I) combine an Aerodyne quantum cascade laser spectrometer for $CO_2$ isotopes with an LI-8100A/8150 automated closed-chamber system, (II) deploy the system under field conditions in a forest ecosystem to yield high-frequency measurements of $\delta^{13}C$ of chamber $CO_2$ flux measurements from tree stems, tree roots, intact soil and trenched soil and (III) quantify the

dependence on measured $\delta^{13}C$ of water vapour in the sample air and on the varying $CO_2$ concentrations during chamber measurements to yield accurate $\delta^{13}C$ measurements.

## 2. Materials and Methods

### 2.1. Site Description

Measurements were performed at the Danish Integrated Carbon Observation System Research Infrastructure (ICOS RI) site DK-Sor at 40 meters above sea level (55°29′13″ N, 55°28′45″ E), where tower-based eddy covariance measurements have been made since 1996. A dense forest consisting mostly of European beech (*Fagus sylvatica* L.) covers the site. The climate is temperate maritime with an annual mean temperature of 8.5 °C and an annual mean precipitation of 564 mm. For a comprehensive description of the site see References [27,28].

### 2.2. Measurements of Soil, Root and Stem Respiration

Respiration from intact soil, trenched soil, coarse tree roots and tree stems was measured by automated closed-chambers controlled by a LI-8100A Automated Soil $CO_2$ Flux System connected to a LI-8150 Multiplexer (LI-COR Environmental, Lincoln, NE, USA), which allowed for automated sequential measurements of each of the chambers. Eight 4 L opaque soil chambers each measured soil $CO_2$ flux at circular soil collars with a diameter of 20 cm that were permanently inserted 4 cm into the soil. The soil collars contained soil and litter but no aboveground plant parts. Three of the soil chambers were 8100-101 Long-Term $CO_2$ flux chambers and five were 8100-104 Long-Term $CO_2$ flux chambers (LI-COR Environmental, Lincoln, NE, USA). A trenching was performed on 6 April 2016 to remove the contribution of autotrophic root respiration to the total $R_{soil}$ from four of the plots. The soil was vertically cut to a depth of 25 cm in a circle around four of the eight soil chambers using a spade. Large roots were cut with a saw. To prevent ingrowth of roots over time, a re-trenching was performed monthly.

Root and stem respiration were measured with two custom-made root chambers and two custom-made stem chambers, respectively, similar to the chambers used in Reference [29]. These chambers did not open between measurements. Instead they were continuously flushed with atmospheric air at a flowrate of 1 L $min^{-1}$ between measurements, which resulted in ambient atmospheric $CO_2$ concentration in the chambers. A 10 cm tube, with a filter in the end, was attached to the chamber which acted as a vent to the atmosphere.

The root chambers were made of transparent acrylic glass and were cylindrical in shape with an inner length of 24 cm and an inner diameter of 7 cm, giving a volume of 923 $cm^3$. The chambers were installed in June 2015. For each chamber, a coarse root with a diameter of about 0.5 cm was carefully exposed from a depth of 5–10 cm and rinsed with tap water. The cylinder was made of two halves that allowed the root to be enclosed intact in the chamber. The holes in each end of the cylinder, where the root went through, were sealed with Blu-tack. Following this, the chambers were covered in soil.

The stem chambers were cylindrical in shape and made of opaque polypropylene, with an inner diameter of 15 cm and an inner height of 10 cm, giving a volume of 1757 $cm^2$. They were attached to the stem surfaces at a height of 1.3 m by a rubber extrusion with a u-profile that was attached to the chamber and sealed with silicone. Each chamber was held in place on the stem by an adjustable nylon strap.

### 2.3. Combining the Aerodyne Laser Spectrometer with the Li-8100A/8150

We combined the Aerodyne Single Continuous Wave Quantum Cascade Laser Trace Gas Analyzer for $CO_2$ ($\delta^{13}C$ and $\delta^{18}O$) Isotopes (the Mini Laser Trace Gas Monitor, Aerodyne Research Inc. 45 Manning Road Billerica, MA), henceforth called the QCL system, with the LI-COR LI-8100A/8150 system in a parallel loop on the outlet side of the LI-COR system in accordance with Application note 138 [30]. See Figure 1 for setup. Thus, the flow to and from the laser to the LI-8100A/8150 was

introduced as a sub loop between the LI-8100A and LI-8150. The nominal flowrate between the LI-8100A and LI-8150 is 1.5 to 1.7 L $min^{-1}$. The precision of $\delta^{13}C$ for the QCL system was analysed by the manufacturer. The Allan deviation was 0.062, 0.023 and 0.013‰ for an integration time of 1, 10 and 100 s, respectively. The QCL system was placed in an air-conditioned cabin in the forest where the temperature was kept constant at 20 °C, while the LI-8100A/8150 was placed 10 m outside the cabin. The pressure in the QCL system cell was kept at a pressure below ambient (30 Torr in this case, controlled with a flow controller by the QCL system valve), while the pressure in the LI-8100A/8150 was kept at ambient. A Pfeiffer Vacuum MVP 070-3 pump (Pfeiffer Vacuum GmbH) was connected to the QCL system outlet, which drew air through the QCL system at a flow rate of 1.0 L $min^{-1}$, that is, slightly lower that the nominal flowrate between the LI-8100A and LI-8150. The lower flow rate to the QCL system is required to prevent "back-looping" of output air from the QCL system into the sub loop, which could cause time-delays in the signal of the QCL system compared to the LI-8100A. The closed-chamber method requires an air-tight system. However, introducing another loop with a heavy pump can potentially cause leaks, thereby biasing the measurements. We therefore tested for leakage in the system by performing a soil chamber measurement where the soil collar was sealed by plastic. The Pfeiffer pump and the QCL system were placed inside the cabin, at a time when the $CO_2$ concentration in the cabin was high (≈1000 ppm). If the system was leaky, this would result in an increase in $CO_2$ concentration in the system over time. Following careful fitting and tightening of the tube fittings to and from the pump, a constant ambient $CO_2$ concentration in the system was achieved, indicating a non-leaky system.

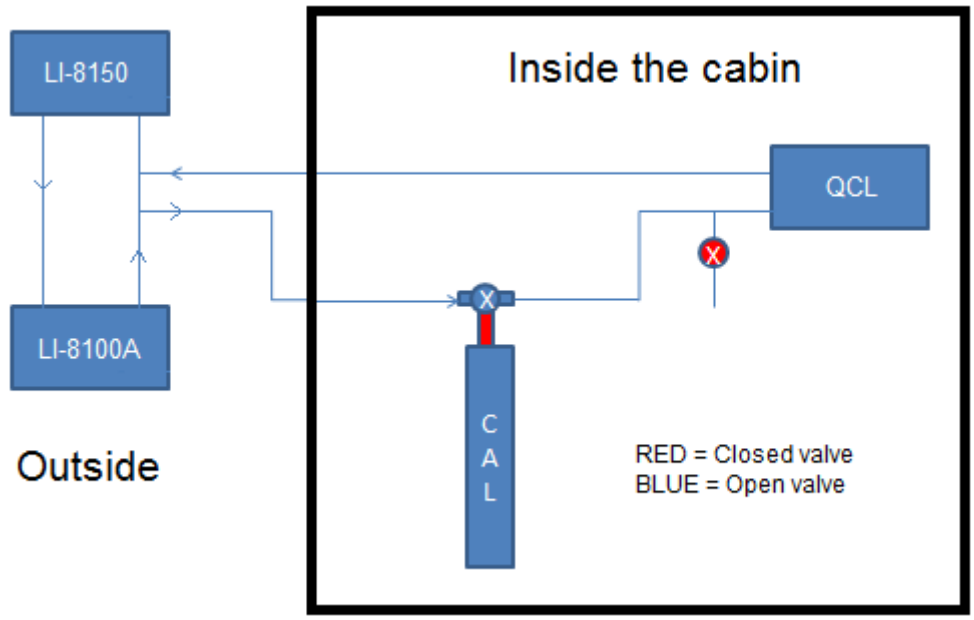


**Figure 1.** Setup of the QCL system and the Li-8100A/8150. The QCL system and calibration gas cylinder (marked "CAL") were placed inside the cabin and the LI-8100A and LI-8150 were placed outside. The setup is shown with the position of the valves during a chamber measurement. See Sections 2.3 and 2.4 for a further description.

### *2.4. Measurement Protocol*

A measurement campaign using the LI-8100A/8150 system combined with the QCL system was made from 6 June to 15 August 2016. For the campaign, the system was set up in a repeated automated two-hour cycle during which a measurement of each of the intact soil, trenched soil, coarse root and stem chambers was performed, followed by a calibration of the QCL system. The chamber enclosure time was set to 5 min and pre-purge and post-purge were both set to 40 s. During the last 12 min of each two-hour measurement cycle, an automatic calibration of the QCL system was performed. The

calibration was performed with a sample of atmospheric air supplied by a 50 L gas cylinder (AGA A/S, Copenhagen, Denmark). A single calibration gas was used, following the recommendation from the QCL system manufacturer. The $\delta^{13}C$ of the calibration gasses were determined by IRMS (Gasbench in continuous flow mode with a Delta V PLUS, Thermo Scientific, Bremen, Germany) at the Laboratory for Stable Isotopes in soil, plant and air at the University of Copenhagen. Working standards for the IRMS analysis were two mixtures of synthetic air with $CO_2$ at near ambient concentration certified at −2.7 (‰ vs PDB) and −29.3 (‰ vs PDB), respectively, supplied by Air Liquide (Air Liquide, Høje Taastrup, Denmark). The $\delta^{13}C$ of the four calibration gases were −10.05, −9.47, −9.39 and −10.48‰, respectively and the average deviation of the gas analysis was <0.2‰. The $CO_2$ concentrations ranged from 390 to 410 ppm. The calibration gas cylinder was connected to the laser inlet tube with a three-way solenoid valve (Figure 1). During normal chamber measurements, the valve from the gas cylinder was closed, thus keeping the closed loop between the QCL system the Li-8100A/8150. During calibration, the valve switched such that the gas from the cylinder was directed to the QCL system inlet. Furthermore, a normally closed one-way solenoid valve in a tee before the QCL system inlet opened as well. This opened the closed loop and provided an overflow of any access gas from the gas cylinder (Figure 1). The timing of opening and closing of the valves was controlled by the QCL system TDL Wintel software (version 14.92, Aerodyne Research Inc., Billerica, MA, USA). The first 80 s of the calibration were set as a flush time, followed by 20 s used to obtain data for the calibration. Following this, the valves switched back to normal operation and a new two-hour cycle could begin.

### 2.5. Test for Water Vapour and $CO_2$ Concentration Dependence

To allow for accurate and un-biased measurements of $\delta^{13}C$, the effect of sample water vapour and absolute $CO_2$ concentration on the measured $\delta^{13}C$ was determined.

The mixing ratios of the isotopologues $^{16}O^{12}C^{16}O$ and $^{16}O^{13}C^{16}O$ measured by the QCL system are reported by the TDL Wintel software following the high-resolution transmission molecular absorption database (HITRAN) notation as 626 and 636, respectively, which are scaled by standard isotopic abundances in ppb [31]. We will use the HITRAN notation in this paper. The effect of water vapour on measured 626 and 636 was determined by varying the water vapour content in a gas from a gas cylinder with a known $\delta^{13}C$ (−24.47‰, determined by IRMS). We constructed a system where part of the gas from the gas cylinder could pass through a 20 L blue cap bottle containing tap water (a water bubbler) and part of the gas could bypass the water bubbler, controlled by two restriction valves before the air was let to the laser inlet. By varying the amount of gas that passed through the water bubbler, different water vapour contents of the gas could be made ranging from 0 mmol $mol^{-1}$ (completely bypassing the water bubbler) to 20 mmol $mol^{-1}$ (all gas passing through the water bubbler). This spanned the concentration range of water vapour during the chamber measurements that typically was between 10 to 15 mmol $mol^{-1}$. The QCL system does not measure the water vapour content of the air. Thus, we connected a LI-7000 infrared gas analyser (LI-COR Environmental, Lincoln, NE, USA) to the outlet of the QCL system to measure water vapour concentration. The results were used to calculate the water vapour dilution effect and the vapour pressure line broadening (VPB) correction coefficient ($\alpha_v$). From this we derived an equation to calculate the dry mixing ratios 626 and 636, which we then used to calculate the dry $\delta^{13}C$ corrected for water vapour.

The dependence of sample $CO_2$ concentration on measured $\delta^{13}C$ was determined by varying the $CO_2$ concentration while keeping the $\delta^{13}C$ constant in a dry gas from a cylinder of known $\delta^{13}C$. The gas had a $CO_2$ concentration of 1590 ppm and a $\delta^{13}C$ of −24.5‰ (determined by IRMS). Samples with different $CO_2$ concentrations were made by mixing the gas of known $\delta^{13}C$ with $CO_2$ free synthetic air from a gas cylinder into a 20 L plastic bag. The $CO_2$ concentration and $\delta^{13}C$ of the sample were then measured by placing the QCL system inlet tube in the plastic bag. Different mixes ranging from 350 ppm to 1590 ppm were made during a 3-h experiment. The relationship between measured $\delta^{13}C$ and the $CO_2$ concentration of the sample was quantified by linear regression.

### 2.6. Data Analysis

All data analysis was performed in R version 3.2.0 [32]. From the raw QCL system data of 626 and 636, a corrected $\delta^{13}C$ was calculated from the calibration with the gas of known $\delta^{13}C$ and by including the experimentally determined impact of $CO_2$ concentration and water vapour of the sample on the measured mixing ratios of 626 and 636. Subsequently, the $\delta^{13}C$ of the $CO_2$ for each chamber measurement was determined by the Keeling plot method.

For each chamber measurement, the data from the initial period of 120 s after chamber closure was discarded (the dead band) from further analysis. This relative long dead band was necessary to ensure adequate mixing of air between the QCL system and the LI-8100A/8150 system.

The mixing ratios of 626 and 636 were corrected based on the empirically determined effects of water vapour on the measured mixing ratios (see Section 3.1.). From this, the dry $\delta^{13}C$ corrected for water vapour was calculated in accordance with TDL Wintel manual as

$$\delta^{13}C_{dry} = \left( \frac{\chi_{636}^{\text{dry}}}{\chi_{626}^{\text{dry}}} - 1 \right) 1000 \quad (1)$$

where $\chi_{636}^{\text{dry}}$ and $\chi_{626}^{\text{dry}}$ are the dry mixing ratios of 636 and 626, respectively. In the second step, the $\delta^{13}C$ was corrected for the effect of sample $CO_2$ concentration based on the empirical relationship observed between $CO_2$ concentration and measured $\delta^{13}C$. The $\delta^{13}C$ was normalised to a $CO_2$ concentration of 400 ppm. Finally, the fully corrected $\delta^{13}C$ was calculated by correcting for the difference in the measurement of calibration gas $\delta^{13}C$ between the QCL system and the IRMS. During the measurement campaign, the calibration gas was measured every two hours and linear interpolation between two adjacent calibrations was used to get a specific $\delta^{13}C$ calibration value at any given time between calibrations, that is, during chamber measurement. From the fully corrected $\delta^{13}C$ values, the $\delta^{13}C$ of the $CO_2$ flux was determined for each chamber measurement by applying the Keeling plot method [10]. This means that for each chamber measurement, the fully corrected $\delta^{13}C$ was fitted against the reciprocal dry $CO_2$ concentration by linear regression and the $\delta^{13}C$ of the $CO_2$ flux was determined as the intercept with the y-axis from the linear regression. The Keeling plot method was also used on $\delta^{13}C$ data where no calibrations had been applied to the measured $\delta^{13}C$, where $\delta^{13}C$ had been calibrated against the calibration gas and where only the $CO_2$ concentration dependence correction had been applied, respectively, to examine the individual effects of the corrections on the final $\delta^{13}C$ determined by the Keeling plots. A $CO_2$ flux was calculated as well for each measurement on a time and soil, root or stem surface area basis by applying a linear regression to the increase in chamber $CO_2$ concentration during chamber closure time similarly to Reference [33].

$\delta^{13}C$ values determined by the Keeling plots were removed from further analysis if the difference in the raw measured $\delta^{13}C$ values between two adjacent calibrations was higher than 2.5‰. This was done to discard data from periods when internal drift in the QCL system was high. In addition, data were discarded from further analysis if the linear Keeling plot regression produced $R^2 < 0.90$. Flagging of data with an $R^2$ value lower than 0.9 of the linear Keeling plot regression, removed 662 (8.4%) of the measurements and flagging of data with a difference in the $\delta^{13}C$ value higher than 2.5‰ between the calibrations made every two hours removed 593 (7.6%) of the data. This left 6588 chamber measurements for the two-month measurement campaign.

From the remaining $\delta^{13}C$ values determined by the Keeling plots, the data was investigated to examine differences between plots and variation in $\delta^{13}C$ on a seasonal and diel timescale. The mean $\delta^{13}C$ for the entire two-month measurement period as well as the diel pattern of $\delta^{13}C$ were calculated for each plot in the following way. First, the mean $\delta^{13}C$ was calculated for each of the 12 times of the day. This provided the diel pattern $\delta^{13}C$ across the day. Then, the mean daily $\delta^{13}C$ for each plot was calculated from the 12 $\delta^{13}C$ values.

## 3. Results

### *3.1. Water Vapour and $CO_2$ Concentration Dependence*

The measured mixing ratios of 626 and 636 were lower in wet compared to dry air and water vapour affected the two species differently resulting in a negative relationship between measured $\delta^{13}C$ and water vapour concentration (Figure 2). The results were used to parameterise the equation for the VPB correction coefficient for both species, which we could use to calculate the dry mixing ratios of a sample containing water vapour:

$$\chi_{626}^{\text{dry}} = (1 + \alpha_{v626} \times \chi_{\text{H2O}}) \times \chi_{626} \quad (2)$$

and

$$\chi_{636}^{\text{dry}} = (1 + \alpha_{v636} \times \chi_{\text{H2O}}) \times \chi_{636} \quad (3)$$

where $\alpha_{v626}$ and $\alpha_{v636}$ are the experimentally determined VPB correction coefficients of 0.006092 1000/mol $H_2O$ and 0.007694 1000/mol $H_2O$ for 626 and 636, respectively. $\chi_{\text{H2O}}$ is the measured content of water vapour in the sample in ‰ and $\chi_{626}$ and $\chi_{636}$ are the measured raw mixing ratios of 626 and 636 from the QCL system, respectively, in ppb following the HITRAN notation. The dilution effect accounts for 1 (mol $H_2O$)$^{-1}$ and the line broadening effect is thus 5.092 and 6.694 (mol $H_2O$)$^{-1}$ for $\chi_{626}$ and $\chi_{636}$, respectively. The extra effect from pressure line broadening would under the field conditions, where $\chi_{\text{H2O}}$ ranged between 10 and 15‰, account for 6.1 to 9.1% for $\chi_{626}$ and 7.7 to 11.5% for $\chi_{636}$.

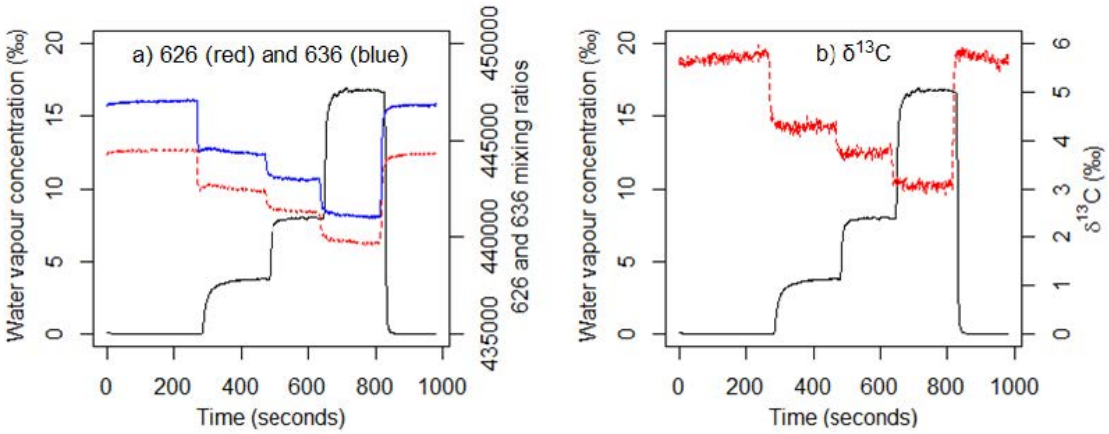


**Figure 2.** Effect of water vapour concentration on the measured mixing ratios of 626 and 636 and the resulting $\delta^{13}C$. (**a**) The effect of water vapour concentration (black line) on measured 626 (red line) and measured 636 (blue line). (**b**) The effect of water vapour (black line) on measured $\delta^{13}C$ (red line). The figures show an example from the experiment where the water vapour concentration was varied in a gas from a gas cylinder, that is, the $\delta^{13}C$ of the sample remained constant.

The experiment to test the effect of sample $CO_2$ concentration on the measured $\delta^{13}C$ values, that is, when the $\chi_{626}$ was changed and the $\delta^{13}C$ was kept constant, showed a negative relationship between $CO_2$ concentration and measured $\delta^{13}C$ (Figure 3). We used linear regression to describe this relationship (intercept: −8.1024, slope: $-5.405 \times 10^{-6}$, $R^2 = 0.71$), which corresponded to a decrease in $\delta^{13}C$ of 0.54‰ per a 100 ppm increase in $CO_2$ concentration. We used the intercept and slope to derive the equation:

$$\delta^{13}C_{dry,\ H2Ocorr} = \left(-5.405 \times 10^{-6} \times \chi_{626}^{\text{dry}} - 8.1014 - \delta^{13}C_{ref}\right) + \delta^{13} \quad (4)$$

which was used to normalise the $\delta^{13}C$ to a $CO_2$ concentration of 400 ppm, at which $CO_2$ concentration the true $\delta^{13}C$ was known from the calibration gas. $\delta^{13}C_{ref}$ is the $\delta^{13}C$ at a $\chi_{626}^{\text{dry}}$ of 400000 ppb (400 ppm $CO_2$) and $\delta^{13}C_{dry}$ is the $\delta^{13}C$ after being corrected for water vapour.

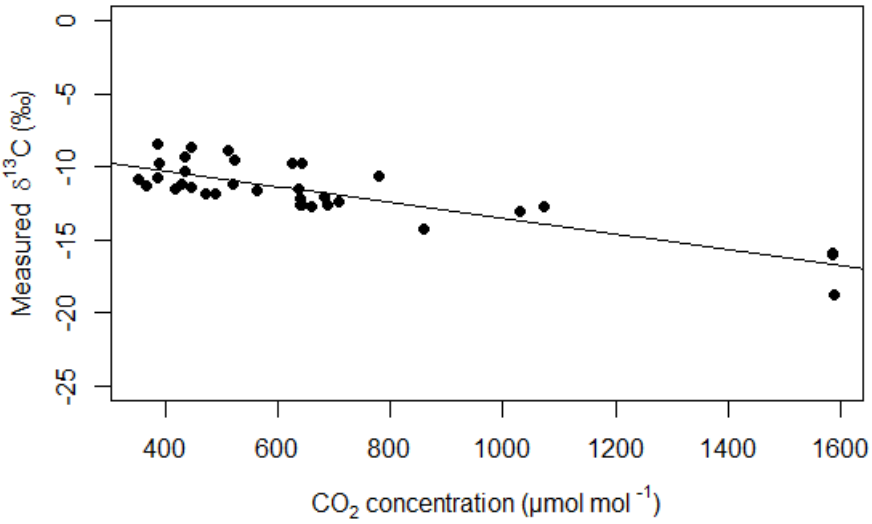


**Figure 3.** Effect of the $CO_2$ concentration dependence on measured $\delta^{13}C$ determined by the QLC. The points show the measurements of the samples with different $CO_2$ concentrations that were made by mixing a gas of known $\delta^{13}C$ with $CO_2$ free synthetic air and the line shows the fitted linear regression from which equation (4) was derived.

### 3.2. *Effect of the $\delta^{13}C$ Corrections on the Keeling Plots*

The corrections for water vapour and $CO_2$ concentration dependence were both important but differed in their effect on the Keeling plots of the four different plot types measured with the automated chambers (Figure 4, Table 1).

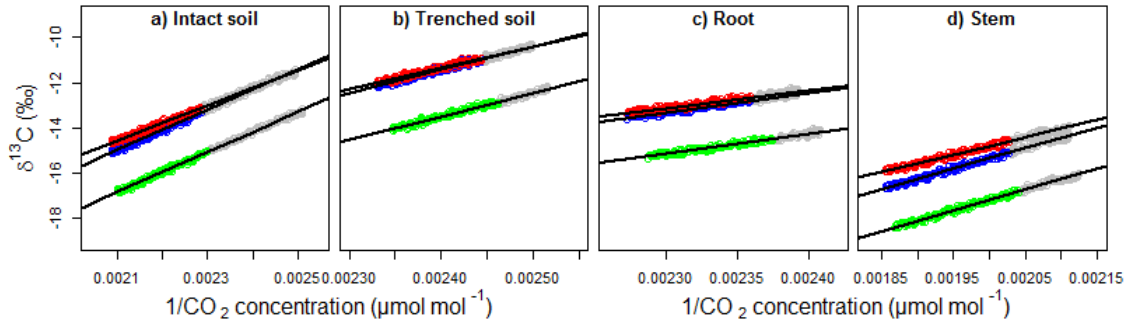


**Figure 4.** Examples of Keeling plots during the automatic chamber campaign for an intact soil measurement (**a**), a trenched soil measurement (**b**), a root measurement (**c**) and a stem measurement (**d**). For each measurement three data series are shown. The green shows the 300 s of raw data for a chamber measurement where no corrections have been applied to the mixing ratios. The blue shows the data where the water vapour correction has been applied and the red shows the data where both the water vapour and the $CO_2$ concentration corrections have been applied. The grey data points for each data series represent data before the dead band of 120 s that were excluded from the Keeling plot. The regression line of the Keeling plot is shown in black for each data series. All the $\delta^{13}C$ values were calibrated against a standard calibration gas with known $\delta^{13}C$.

**Table 1.** The mean Keeling plot intercepts (the determined $\delta^{13}C$ of the $CO_2$ flux) and slopes using the measured $\delta^{13}C$, the $\delta^{13}C$ corrected for water vapour and the $\delta^{13}C$ corrected for both water vapour and $CO_2$ concentration dependence, respectively. The means are shown for all measurements together and individually for intact soil, trenched soil, roots and stems, respectively. All $\delta^{13}C$ values were calibrated against a standard calibration gas with known $\delta^{13}C$.

| Plot Type | Keeling Plot Parameter | Using Measured $\delta^{13}C$ | Using $\delta^{13}C$ Corrected for Water Vapour | Using $\delta^{13}C$ Corrected for Water and $CO_2$ |
|---|---|---|---|---|
| All | Intercept | −35.7 ± 2.9 | −33.6 ± 2.8 | −30.2 ± 2.9 |
| | Slope | 9577 ± 1304 | 9588 ± 1325 | 8164 ± 1329 |
| Intact soil | Intercept | −35.3 ± 2.6 | −33.1 ± 2.6 | −29.8 ± 2.7 |
| | Slope | 9412 ± 1176 | 9370 ± 1172 | 7958 ± 1212 |
| Trenched soil | Intercept | −35.1 ± 2.9 | −32.8 ± 2.8 | −29.7 ± 2.9 |
| | Slope | 9272 ± 1277 | 9251 ± 1265 | 7954 ± 1288 |
| Roots | Intercept | −37.4 ± 3.0 | −35.5 ± 3.0 | −32.6 ± 2.9 |
| | Slope | 10246 ± 1415 | 10415 ± 1433 | 9214 ± 1380 |
| Stems | Intercept | −36.2 ± 2.5 | −34.3 ± 2.5 | −30.2 ± 2.4 |
| | Slope | 9901 ± 1261 | 9959 ± 1279 | 8134 ± 1206 |

Both corrections increased the intercept with the y-axis of the Keeling plots and thus the determined $\delta^{13}C$ estimate of the source of the $CO_2$ flux in all cases. The water vapour correction increased the mean $\delta^{13}C$ for all measurements by 2.1‰ (from −35.7 ± 2.9‰ to −33.6 ± 2.8‰, Table 1), while the additional $CO_2$ concentration dependence correction had a higher effect by increasing the overall mean $\delta^{13}C$ by 3.4‰ (to −30.2 ± 2.9‰). For the water vapour correction, only small differences were seen between the four plot types. In contrast, the $CO_2$ concentration dependence correction had the largest effect on the stem measurements followed by the intact soil, trenched soil and roots, yielding increases of the measured $\delta^{13}C$ of 4.1, 3.3, 3.1 and 2.9‰, respectively. No change was seen in the slope of the Keeling plot from the water vapour correction (Table 1). This contrasted with the $CO_2$ concentration dependence correction, which on average decreased the slope by 14.9% (from 9588 ± 1325 to 8164 ± 1329). The biggest decrease was seen for the stem chambers, followed by the intact soil, trenched soil and root chambers, which decreased by 18.3, 15.1, 14.0 and 11.5%, respectively.

The $\delta^{13}C$ of the standard calibration gases varied from −10.48 to −9.39‰ as measured by IRMS. The $\delta^{13}C$ measured by the QCL system during the calibrations was, however, on average 17.85‰ lower than the $\delta^{13}C$ of the standard gases, with a standard deviation of 1.19. Thus, in the final step of the calibration, on average 17.85‰ was added to the $\delta^{13}C$ corrected for water vapour and $CO_2$ concentration dependence to give the fully calibrated absolute value of $\delta^{13}C$.

### 3.3. Automated Chamber Measurement Campaign

Both the $CO_2$ fluxes and the $\delta^{13}C$ of the $CO_2$ fluxes showed considerable variation over time (Figure 5).

To compare the $\delta^{13}C$ of the $CO_2$ flux from the four different plot types, we calculated the mean $\delta^{13}C$ for each of the 12 plots (Figure 6). The mean $\delta^{13}C$ for all plots was −30.3 ± 1.3‰. The mean $\delta^{13}C$ for intact soil plots was −29.8 ± 0.32‰ with only small differences between the four plots. The $\delta^{13}C$ for the trenched soil plots was similar to the intact soil plots with a mean $\delta^{13}C$ of −29.8 ± 1.2‰. One of the trenched soil plots (Trenched soil 4), however, had a $\delta^{13}C$ of −28.0 ± 0.32‰, higher than any of the $\delta^{13}C$ for the intact soil plots, while the other three trenched soil plots had a mean $\delta^{13}C$ of −30.4 ± 0.41‰, slightly lower than the intact soil plots. The two root plots had the lowest $\delta^{13}C$ of all plots with $\delta^{13}C$ values of −33.1 ± 0.88‰ and −32.0 ± 0.35‰ for Root 1 and Root 2, respectively, resulting in a mean $\delta^{13}C$ of −32.6 ± 0.78‰. Finally, the two stem plots showed $\delta^{13}C$ values of −30.7 ± 0.28‰ and

−29.7 ± 0.43‰ for Stem 1 and Stem 2, respectively, resulting in a mean $\delta^{13}C$ of −30.2 ± 0.74‰, which was similar to the mean $\delta^{13}C$ of the trenched plots.

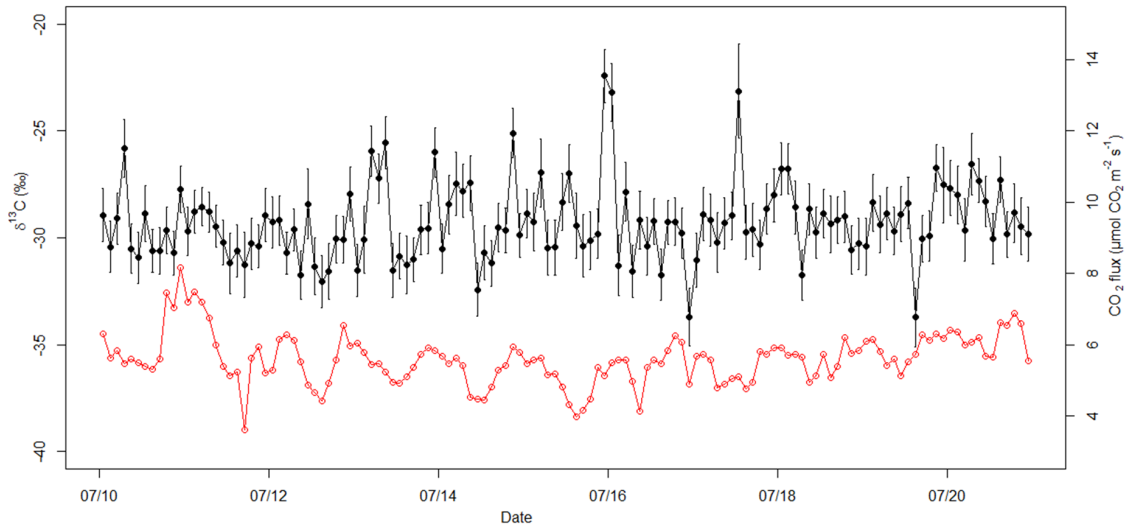


**Figure 5.** Example of 10 days of continuous, bi-hourly closed-chamber measurements from 10 July to 21 July for an intact soil plot. Both the $\delta^{13}C$ of the $CO_2$ fluxes determined by Keeling plots (black points and line) and the $CO_2$ fluxes (red circles and line) are shown. Error bars on $\delta^{13}C$ values show ± standard deviation of the intercept from the linear Keeling plot regression.

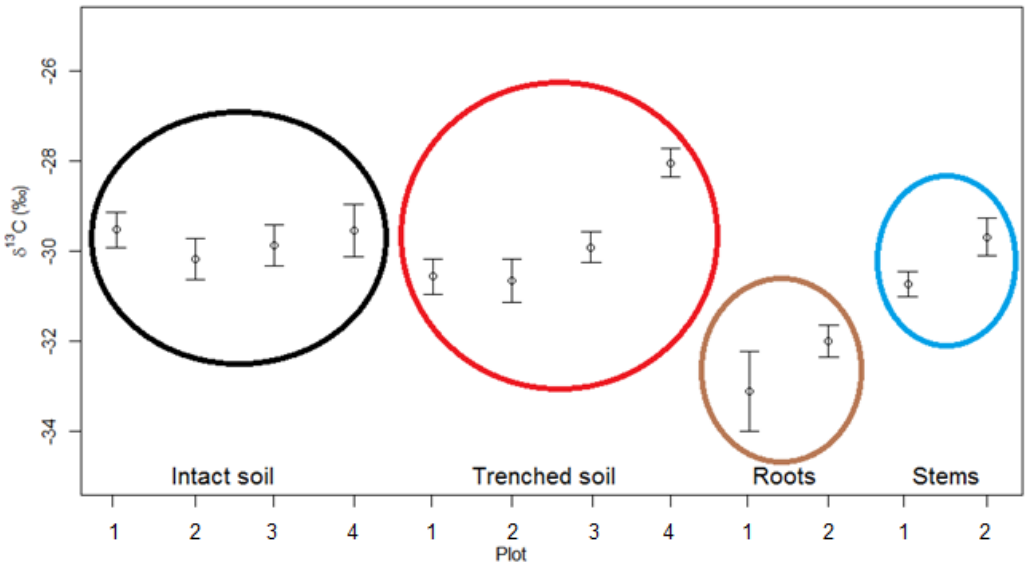


**Figure 6.** Mean $\delta^{13}C$ of the $CO_2$ fluxes determined by Keeling plots (± standard deviation) for each of the 12 plots throughout the measurement period. The plots are shown from left to right in the following order: Intact soil 1, 2, 3 and 4. Trenched soil 1, 2, 3 and 4. Root 1 and 2 and Stem 1 and 2.

$CO_2$ flux measurements with the LI-8100A/8150 system had been performed since January 2016 [29]. This allowed for examining the effect of trenching on the $CO_2$ fluxes, by looking at the $CO_2$ fluxes from the intact and trenched plots in January, February and March, before the trenching on 6 April and during the laser campaign in June, July and August. For January, February and March, the trenched plot 1, 2, 3 and 4 accounted for 70.9, 83.9, 119.5 and 100.9%, respectively, of the mean $CO_2$ flux for the intact soil plots. However, during the QCL system measurement campaign they only accounted for 55.5, 62.4, 91.6 and 91.4%, respectively, corresponding to a decrease relatively to the intact soil plots of 21.7, 25.6, 23.4 and 9.4%, respectively.

The mean $\delta^{13}C$ for each plot was based on two months of measurements. Thus, to examine the consistency of the mean throughout the measurement campaign and to see if any day to day variability and seasonality was present (Figure 7), we looked at $\delta^{13}C$ as well as the $CO_2$ fluxes for each plot throughout the entire period. The intact soil, trenched soil and stem plots generally showed an increase in $CO_2$ fluxes during the first quarter of the measurement period, followed by a period of high fluxes and finally lower fluxes again by the end of the measurement period. This temporal pattern followed the soil temperature measured at 5 cm depth (Figure 8). The two root plots differed; however, by showing two peak periods of $CO_2$ fluxes during the measurement period (Figure 7i,j). In contrast to the $CO_2$ fluxes, $\delta^{13}C$ showed no clear pattern across the two months. The $\delta^{13}C$ for each plot did, however, show some day to day variability, with $\delta^{13}C$ values typically ranging within 2–3‰ depending on plot.

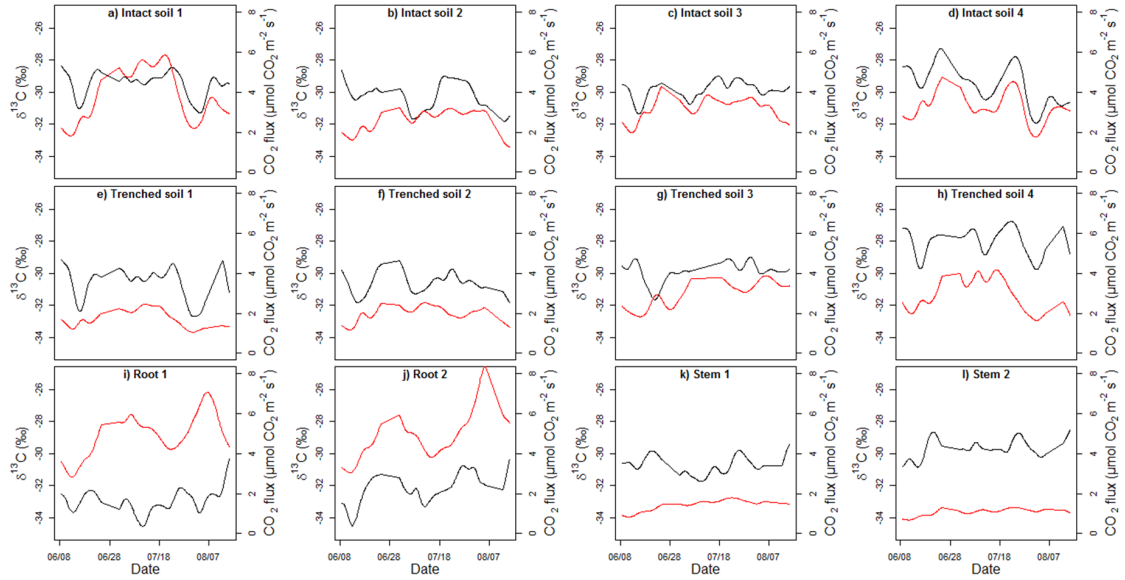


**Figure 7.** $\delta^{13}C$ of the $CO_2$ fluxes determined by Keeling plots (black lines) and the $CO_2$ fluxes (red lines) for each of the plots throughout the measurement period. $\delta^{13}C$ and $CO_2$ fluxes are each shown as rolling averages of the daily means. (**a**–**d**) Intact soil 1 to Intact soil 4. (**e**–**h**) Trenched soil 1 to Trenched soil 4. (**i**,**j**) Root 1 and Root 2, respectively. (**k**,**l**) Stem 1 and Stem 2, respectively.

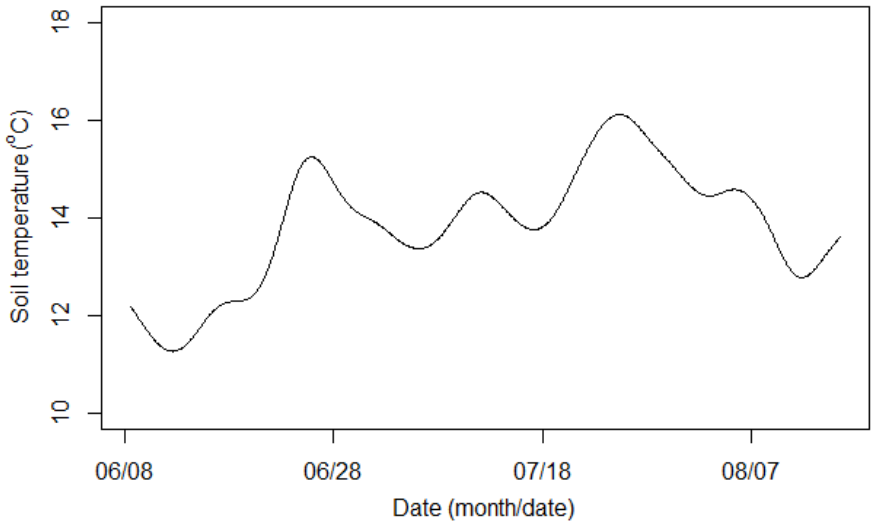


**Figure 8.** Soil temperature measured at 5 cm depth throughout the measurement period. The soil temperature probe was placed close to the chamber plots, with all plots being within a distance of 10 m. A rolling average has been applied to the raw soil temperature measurements.

For a few plots (e.g., intact soil 4, Figure 7d), an apparent relationship between the $CO_2$ flux and $\delta^{13}C$ was seen, with higher $CO_2$ fluxes resulting in higher $\delta^{13}C$ values. To examine this further, we performed a linear regression between $CO_2$ flux and $\delta^{13}C$ for each plot. We also performed a linear regression between soil temperature at 5 cm depth and $\delta^{13}C$. A significant positive linear relationship was found between $CO_2$ flux and $\delta^{13}C$ for all plots, except Trenched soil 3 and Root 1. $R^2$ values were, however, generally low (Table 2). For soil temperature and $\delta^{13}C$, a significant positive relationship was only found for five plots. As for $CO_2$ flux and $\delta^{13}C$, $R^2$ values were low.

**Table 2.** Results of the linear regressions between the $CO_2$ fluxes and $\delta^{13}C$ of the $CO_2$ fluxes and the linear regressions between the soil temperature at 5 cm depth and $\delta^{13}C$ of the $CO_2$ fluxes for each plot. For each regression, the adjusted $R^2$, slope and *p*-value are shown. A *p*-value in bold indicate a significant *p*-value.

| Plot | $CO_2$ Flux and $\delta^{13}C$ | | | Soil Temperature and $\delta^{13}C$ | | |
|---|---|---|---|---|---|---|
| | Adjusted $R^2$ | Slope ± SE | *p*-Value | Adjusted $R^2$ | Slope ± SE | *p*-Value |
| Intact soil 1 | 0.051 | 0.41 ± 0.071 | **<0.001** | −0.00071 | 0.059 ± 0.077 | 0.45 |
| Intact soil 2 | 0.04 | 0.81 ± 0.16 | **<0.001** | 0.0071 | 0.18 ± 0.080 | **<0.05** |
| Intact soil 3 | 0.043 | 0.66 ± 0.13 | **<0.001** | 0.0071 | 0.18 ± 0.075 | **<0.05** |
| Intact soil 4 | 0.15 | 0.93 ± 0.085 | **<0.001** | 0.0003 | −0.081 ± 0.074 | 0.276 |
| Trenched soil 1 | 0.054 | 1.4 ± 0.26 | **<0.001** | −0.002 | −0.010 ± 0.098 | 0.92 |
| Trenched soil 2 | 0.033 | 0.98 ± 0.27 | **<0.001** | 0.01 | 0.22 ± 0.089 | **<0.05** |
| Trenched soil 3 | −0.0019 | 0.11 ± 0.19 | 0.56 | −0.0012 | 0.096 ± 0.13 | 0.45 |
| Trenched soil 4 | 0.048 | 0.44 ± 0.080 | **<0.001** | −0.0013 | 0.038 ± 0.071 | 0.59 |
| Root 1 | 0.04 | 0.42 ± 0.090 | **<0.001** | −0.0018 | 0.035 ± 0.11 | 0.74 |
| Root 2 | 0.052 | 0.50 ± 0.10 | **<0.001** | 0.023 | 0.37 ± 0.11 | **<0.01** |
| Stem 1 | −0.0016 | 0.018 ± 0.27 | 0.95 | −0.0014 | 0.025 ± 0.062 | 0.68 |
| Stem 2 | 0.0056 | 1.0 ± 0.49 | **<0.05** | 0.0072 | 0.16 ± 0.071 | **<0.05** |

We calculated the mean diel pattern of $\delta^{13}C$ and $CO_2$ fluxes for the entire measurement period for each plot (Figure 9). For the intact soils (Figure 9a–d) and the trenched soils (Figure 9e–h), the $CO_2$ fluxes were generally higher during the night-time than during daytime. Root 1 and the stem plots, however, showed the highest fluxes during daytime, while Root 2 showed the highest fluxes between 04:00 and 08:00 CET. The diel pattern of $\delta^{13}C$ showed a larger variation within groups than the $CO_2$ fluxes. $\delta^{13}C$ for a plot was generally within a 1–3‰. For some plots no apparent diel pattern was observed (Intact soil 3, Trenched soil 1, Trenched soil 3, Root 2, Stem 1 and Stem 2). The remaining plots, however, showed varying degrees of diel fluctuation. Intact soil 1, 2 and 4 showed highest $\delta^{13}C$ values during night-time and lowest $\delta^{13}C$ values during daytime. The difference between the daytime average (09:00 to 15:00 CET) and night-time average (21:00 to 03:00 CET) was 0.65, 0.93 and 0.92‰ for Intact soil 1, 2 and 4, respectively, with Intact soil 4 showing the largest difference of 1.98‰ between two hours of the day (−28.4‰ at 04:00 CET and −30.4 at 08:00 CET). Trenched soil 2 showed a moderate diel pattern similar to the intact soil plots, with the lowest $\delta^{13}C$ of −31.4‰ at 10:00 CET and the highest $\delta^{13}C$ of −30.0‰ at 00:00 CET. The diel pattern of $\delta^{13}C$ for Trenched soil 4 differed by showing the highest $\delta^{13}C$ values late in the afternoon and the lowest $\delta^{13}C$ values early in the morning, with the highest and lowest $\delta^{13}C$ values of −27.5 and −28.6‰ at 16:00 and 06:00 CET, respectively. Root 1 showed the largest diel pattern of any plot with the lowest $\delta^{13}C$ of −34.7‰ seen at 04:00 CET. From 04:00 CET, $\delta^{13}C$ increased until 10:00 CET (a $\delta^{13}C$ of −32.1‰) and remained high until 18:00 CET (a $\delta^{13}C$ of −32.0‰).

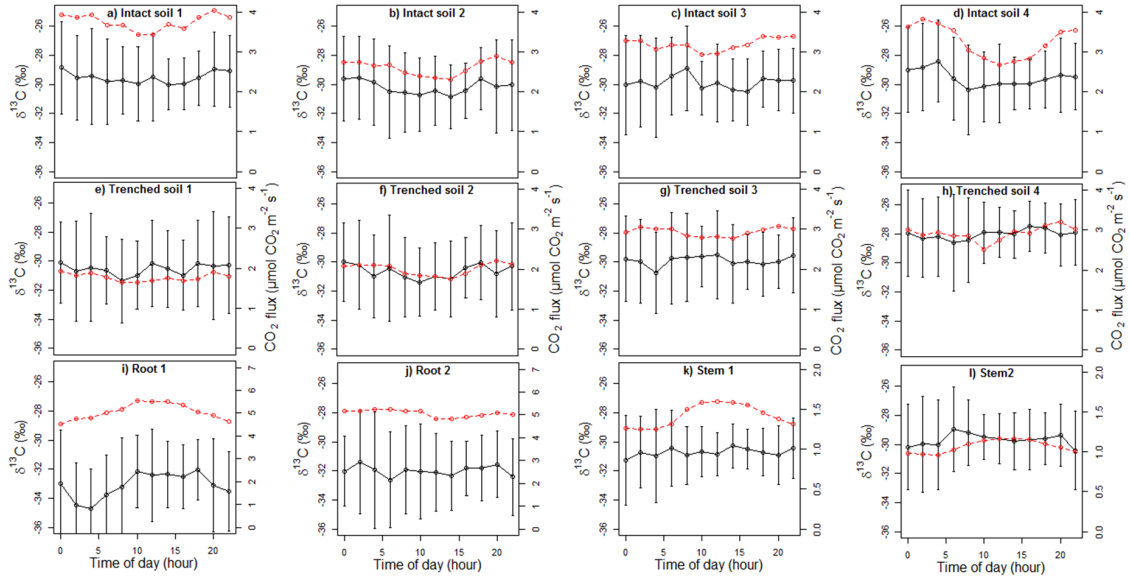


**Figure 9.** Diel patterns of $\delta^{13}C$ of the $CO_2$ fluxes determined by keeling plots (± standard deviation, black points and lines) and the $CO_2$ fluxes (red circles and lines), based on bi-hourly means throughout the measurement period for each of the 12 plots. (**a**–**d**) Intact soil 1 to Intact soil 4. (**e**–**h**) Trenched soil 1 to Trenched soil 4. (**I**,**j**) Root 1 and Root 2, respectively. (**k**,**l**) Stem 1 and Stem 2, respectively.

## 4. Discussion

### *4.1. Effect of the $\delta^{13}C$ Corrections*

The corrections for water vapour and $CO_2$ concentration dependence both lowered the $\delta^{13}C$, which consequently lowered the estimated $\delta^{13}C$ of the $CO_2$ fluxes determined by the Keeling plots during the automated closed-chamber campaign (Figure 4, Table 1). Although the $CO_2$ concentration dependence correction only slightly changed the $\delta^{13}C$, it had the largest impact on the $\delta^{13}C$ determined from the Keeling plots, because it changed the slope of the plots. The change in $CO_2$ concentration and $\delta^{13}C$ during a measurement is inherent to the closed-chamber method for determination of the $\delta^{13}C$ of the source by the Keeling plot method. Our results highlight the importance of the $CO_2$ concentration dependence correction, which is likely more important for closed-chamber measurements than, for example, for eddy covariance measurements, where the $\delta^{13}C$ is measured at an atmospheric $CO_2$ concentration with small absolute fluctuation during a flux sample. Direct comparison of our results with previous studies is not possible because no one else has previously combined an Aerodyne $CO_2$ isotope QCL system with the LI8100A/LI8150 system for automated closed-chamber measurements. However, the issues of dependence of water vapour and especially $CO_2$ concentration on measured $\delta^{13}C$ have been addressed in a few studies using laser spectroscopy methods, including quantum cascade lasers [19,23–25,34]. In a study where $\delta^{13}C$ was measured with a quantum cascade laser spectrometer, [21] performed 90 closed-chamber measurements and determined the $CO_2$ concentration dependency but did not report the effect of this calibration on the raw $\delta^{13}C$ values or the effect on the $\delta^{13}C$ determined by the Keeling plots. [18] used an Aerodyne isotope quantum cascade laser spectrometer for eddy covariance measurements and also characterised the instrument's $CO_2$ concentration dependence but likewise did not report the results. [35] compared two cavity ring-down spectroscopy analysers and found an increase in $\delta^{13}C$ per 100 ppm of 0.46 and 0.09‰, respectively, for the two analysers. This is in contrast to our observation of a decrease in $\delta^{13}C$ per 100 ppm of 0.54‰. [36], however, found no concentration dependency of $\delta^{13}C$ in the $CO_2$ concentration range of 303–437 ppm. The same lack of $CO_2$ concentration dependency was found for the quantum cascade laser spectrometer developed by [13]. Taken together, it is clear that large differences in the $CO_2$ concentration dependence between different laser spectroscopy instruments exist. However, the reason

for the concentration dependence remains unresolved [37]. Based on this study and previous studies using laser spectrometers for $\delta^{13}C$ measurements, we recommend quantifying the $CO_2$ concentration dependence for each instrument, for example, by using the approach described in this study.

### 4.2. Overall $\delta^{13}C$ Values of the $CO_2$ Fluxes From Intact Soils, Trenched Soils, Roots and Stems

The $\delta^{13}C$ signatures from heterotrophic and autotrophic $R_{soil}$ have previously been measured at the DK-Sor site using manually taken air samples followed by isotopic analysis by IRMS [38] and the results of the partitioning of soil respiration into heterotrophic and autotrophic components were independently confirmed by [39]. It has been found that $\delta^{13}C$ from heterotrophic respiration of soil organic matter is enriched compared to $\delta^{13}C$ from autotrophic respiration, with the resulting $\delta^{13}C$ of $R_{soil}$ from intact soil falling in between, because it is a mix of heterotrophic and autotrophic respiration [38,40]. This has been used to partition $R_{soil}$ into heterotrophic and autotrophic respiration by applying a linear mixing model, thus providing measurements of process-based fluxes, which can be used to improved process-based $CO_2$ flux models [38]. Ideally, the intact soil plots contain both roots and soil organic matter, whereas the trenched plots do not contain any live roots. The lower root $\delta^{13}C$ compared to both the intact and trenched soil, fits well the generally depleted $\delta^{13}C$ observed for roots [40]. However, we found a similar mean $\delta^{13}C$ for the intact and trenched plots, which disagrees with earlier studies that found higher $\delta^{13}C$ for heterotrophic $R_{soil}$ [41]. The trenched soil plot 4 had a $\delta^{13}C$ of $-28.0 \pm 0.32$‰ and was thus the only plot with a $\delta^{13}C$ higher than the three other trenched plots and the intact soil plots. This is in line with the higher $\delta^{13}C$ observed for soil organic matter. It remains unexplained why we did not see a difference in $\delta^{13}C$ between the three other trenched plots and the intact soil plots. One possibility is an unsuccessful trenching. Examining the $CO_2$ fluxes for the four trenched plots before and after the trenching, suggested a decrease in $R_{soil}$ ranging from 9.4% to 25.6% for the four trenched plots. This is a relative low decrease based on previous studies of the autotrophic contribution to $R_{soil}$ [42–44], which could indicate an unsuccessful trenching. However, it is possible that the high $R_{soil}$ for the trenched plot was due to respiration of root litter from roots severed by the trenching, which was performed only two months prior to beginning of the measurements [45–47]. In a previous study at the site, the $\delta^{13}C$ of the solid material of fine roots, that made up more than a third of the root biomass, was found to be depleted in $\delta^{13}C$ compared to the soil organic matter [38]. Thus, we expect that the decomposition of the fine roots following a trenching would result in an input to $R_{soil}$ of $CO_2$ depleted in $\delta^{13}C$ compared to the $\delta^{13}C$ of $CO_2$ from the decomposition of the remaining soil organic matter.

The mean $\delta^{13}C$ of the two stem plots was $-30.2 \pm 0.74$‰, a value close to the $\delta^{13}C$ of the soil plots but enriched compared to the $\delta^{13}C$ of the root plots. Stem $CO_2$ flux is typically composed of respiration from the stem. However, it has been found that passive diffusion of $CO_2$ out of the stem from water in the xylem that is being transported from the roots to the shoots, can contribute to the stem $CO_2$ flux as well [48]. The $CO_2$ concentration in the soil pores is high, typically several thousand ppm, which leads to $CO_2$ being dissolved in the soil water [49–51]. This water is taken up by the plant, why the xylem can contain dissolved $CO_2$. We expect that the $\delta^{13}C$ of the $CO_2$ dissolved in the soil water reflects the $\delta^{13}C$ of $R_{soil}$. Thus, if a large part of the stem $CO_2$ flux is derived from this dissolved $CO_2$, then the $\delta^{13}C$ of the stem $CO_2$ flux would reflect this. We measured a $\delta^{13}C$ for the stem $CO_2$ flux close to the $\delta^{13}C$ of $R_{soil}$, which indicates that passive diffusion out of the stem of $CO_2$ from $R_{soil}$ could play a major role in the stem $CO_2$ flux at our site.

The mean $\delta^{13}C$ for all plots was $-30.3 \pm 1.3$‰. Values of $\delta^{13}C$ from respired $CO_2$ from forest ecosystems have been found to lie in the range from $-24$ to $-30$‰ [1]. A previous study at the site gave mean values of $-23.6$ to 21.2‰ for different layers of soil organic matter and $-22.2$‰ for roots [38]. Thus, the $\delta^{13}C$ values found in this study are in the lower range of reported literature values and consistently lower than $\delta^{13}C$ values previously determined at the site. The $\delta^{13}C$ values found by [38] were obtained by manual measurements with gas samples being analysed by IRMS. As discussed in Section 4.1, we found the measured $\delta^{13}C$ to be influenced by water vapour and $CO_2$ concentration and

consequently we corrected the measured $\delta^{13}C$. However, failing to accurately correct for these effects will lead to wrong $\delta^{13}C$ values determined from the Keeling plots. It is possible that the different $\delta^{13}C$ values in the two studies were due to instrumental differences, for example, because of the corrections for water vapour and $CO_2$ concentration of QCL system compared to the IRMS where the gas was purified prior to analysis. In some studies, the Keeling plot method has been found to be biased by diffusive fractionation, which can cause nonlinear Keeling plots, thus violating the basic principle of this method [52]. This can lead to a deviation in the determined $\delta^{13}C$ value of the Keeling plot of up to 4‰ [52]. The Keeling plots in this study, however, were highly linear with generally high $R^2$ values and we only used measurements with a $R^2$ value higher than 0.9 in the analysis (Figure 4). Thus, it is unlikely that diffusive fractionation has had a major influence the determined $\delta^{13}C$ values in this study. In addition, there is uncertainty attached to the determined $\delta^{13}C$ value of the Keeling plot even without diffusive fractionation. In an analysis of 146 Keeling plots from 33 different field sites, [53] found a mean standard error for the Keeling plots of 1.2‰.

### 4.3. Seasonality of $\delta^{13}C$ and Correlation with Flux and Temperature

No major change in $\delta^{13}C$ for the different plots was observed during the two-month measurement period. The $\delta^{13}C$ for each plot did, however, show some day to day variability, with $\delta^{13}C$ values typically ranging within 2–3‰, depending on plot (Figure 7). Any change in $\delta^{13}C$ of the respired $CO_2$ from a plot can be due to either a change in $\delta^{13}C$ from a source, for example, a change in $\delta^{13}C$ from bacterial or root respiration or a change in the individual respiratory contribution of each source that make up the $\delta^{13}C$ of a plot [54]. Heterotrophic and autotrophic respiration have been found to respond differently to factors such as temperature and photosynthesis, with root respiration being more temperature sensitive than respiration of soil organic matter [55,56]. To examine the cause for the observed day to day variability in $\delta^{13}C$ across the two months, we tested the relationship between $\delta^{13}C$ and the $CO_2$ flux and the soil temperature, respectively (Table 2). A significant positive relationship was found between $\delta^{13}C$ and soil temperature for two out of four intact soil plots. The two significant relationships are in contrast to what could be expected, if the roots were to respond more to temperature than the heterotrophic organisms. We found the lowest $\delta^{13}C$ of respiration from roots. Thus, if a higher temperature would result in higher root respiration compared to heterotrophic respiration, then we would expect the $\delta^{13}C$ of total $R_{soil}$ in the intact soil plots to decrease. The linear regressions between $\delta^{13}C$ and the $CO_2$ flux were significant for all plots except two. The day to day variation of $R_{soil}$ has often been found to be caused by changes in temperature and photosynthetic input. The higher $\delta^{13}C$ found in relation to $CO_2$ flux in the intact soils, does not support that root respiration represents a larger part of the total $R_{soil}$ at higher fluxes. However, other reasons for the significant relationship between $\delta^{13}C$ and the $CO_2$ flux are possible such as changing pathways or shifts in substrate [57,58].

### 4.4. Diel Patterns of $\delta^{13}C$

The diel patterns of the $\delta^{13}C$ of the $CO_2$ fluxes showed a high degree of variability with a clear diel pattern for some plots, whereas other plots showed no distinct pattern (Figure 9). However, when considering the variability, no significant diel patterns could be identified. Most of the processes that govern the day to day and seasonal variation in $\delta^{13}C$ may also operate on shorter timescales, thereby potentially causing a diel pattern of $\delta^{13}C$. For stems, a distinct diel pattern has been found with highest $\delta^{13}C$ of the $CO_2$ fluxes during daytime [59], whereas the two stems in our study showed no distinct difference between daytime and night-time $\delta^{13}C$ (Figure 9). In contrast, the stem $CO_2$ fluxes showed a clear diel pattern with highest fluxes during daytime. This may be related to higher temperature, as well as to higher diffusion of $CO_2$ out of the stems due to higher upward xylem transport of soil water enriched with $CO_2$ originally produced in the soil [60].

The contribution of root respiration to soil respiration can vary on a diel timescale due to changes in photosynthesis and substrate supply, thereby changing the diel pattern of $\delta^{13}C$ of the $CO_2$ flux from intact soil. Intact soil 1, 2 and 4 indeed showed a diel pattern with highest $\delta^{13}C$ values during night-time

and lowest $\delta^{13}C$ values during daytime. This followed the $CO_2$ fluxes and the general relationship found by linear regression between $\delta^{13}C$ and $CO_2$ flux. The low daytime $\delta^{13}C$ indicates that root respiration contributes relatively more to total $R_{soil}$ at daytime than during night-time. Normally the higher root respiration on a diel timescale would result in higher total $R_{soil}$. We, however, observed the opposite. It is possible that the $CO_2$ flux measurements during night-time observed in our study are overestimated due to occasionally insufficient mixing of air above the soil surface during low atmospheric turbulence conditions leading to apparently high flux estimates [33]. This potential bias may therefore complicate the interpretation of the measured diel patterns.

## 5. Conclusions

We successfully combined an Aerodyne quantum cascade laser spectrometer for $CO_2$ isotopes with an LI-8100A/8150 automated closed-chamber system to yield real-time $\delta^{13}C$ of $CO_2$ fluxes during a two-month field campaign in a Danish beech forest. We generally found lower $\delta^{13}C$ values compared to a previous study at the site and small differences in $\delta^{13}C$ between different ecosystems compartments, that is, intact soil, trenched soil, tree stems and coarse tree roots. Furthermore, by thoroughly testing the instruments, we found that the $\delta^{13}C$ measured by the laser spectrometer was influenced by the water vapour and $CO_2$ concentration of the sample air and we developed a method to correct for these effects to yield accurate measurements of $\delta^{13}C$.

In conclusion, the study showed the potential of using a quantum cascade laser spectrometer to measure $\delta^{13}C$ of $CO_2$ during automated closed-chamber measurements, thereby allowing for high-temporal measurements of isotopic ecosystem $CO_2$ fluxes. It also highlighted the importance of proper correction for water vapour and $CO_2$ concentration of the sample air to get accurate measurements of $\delta^{13}C$.

**Author Contributions:** Conceptualization, All authors; methodology, All authors; software, A.B., K.S.L. and A.I.; validation, A.B. with input from all authors.; formal analysis, A.B. with input from all authors; investigation, A.B., K.S.L., A.I. and P.A.; resources, K.P., K.S.L., A.I. and P.A.; data curation, All authors; writing—original draft preparation, A.B. with input from all authors; writing—review and editing, A.B. with input from all authors; visualization, A.B. with input from all authors; supervision, K.P., A.I. and K.S.L.; project administration, K.P.; funding acquisition, K.P. with input from A.I., K.S.L. and P.A.

**Funding:** This research was funded by the Danish Ministry for Research, Innovation and Higher Education, the Danish Council for Independent Research, grant number DFF–1323-00182.

**Conflicts of Interest:** The authors declare no conflict of interest. The funder had no role in the design of the study; in the collection, analyses or interpretation of data; in the writing of the manuscript or in the decision to publish the results.

## References

1. Bowling, D.R.; Pataki, D.E.; Randerson, J.T. Carbon Isotopes in Terrestrial Ecosystem Pools and $CO_2$ Fluxes. *New Phytol.* **2008**, *178*, 24–40. [CrossRef] [PubMed]
2. Farquhar, G.D.; Ehleringer, J.R.; Hubick, K.T. Carbon isotope discrimination and photosynthesis. *Annu. Rev. Plant Physiol. Plant Mol. Biol.* **1989**, *40*, 503–537. [CrossRef]
3. Park, R.; Epstein, S. Carbon isotope fractionation during photosynthesis. *Geochim. Cosmochim. Acta.* **1960**, *21*, 110–126. [CrossRef]
4. Janssens, I.A.; Lankreijer, H.; Matteucci, G.; Kowalski, A.S.; Buchmann, N.; Epron, D.; Pilegaard, K.; Kutsch, W.; Longdoz, B.; Grünwald, T.; et al. Productivity overshadows temperature in determining soil and ecosystem respiration across European forests. *Glob. Chang. Biol.* **2000**, *7*, 269–278. [CrossRef]
5. Rochette, P.; Hutchinson, G.L. Measurement of Soil Respiration in situ: Chamber Techniques. In *Micrometeorology in Agricultural Systems*; Agronomy Monograph 47; Hatfield, J.L., Baker, J.M., Eds.; American Society of Agronomy, Crop Science Society of America and Soil Science Society of America: Madison, WI, USA, 2005; pp. 247–286.
6. Edwards, N.T.; Riggs, J.S. Automated monitoring of soil respiration: A moving chamber design. *Soil Sci. Soc. Am. J.* **2003**, *67*, 1266–1271. [CrossRef]

7. Koskinen, M.; Minkkinen, K.; Ojanen, P.; Kämäräinen, M.; Laurila, T.; Lohila, A. Measurements of $CO_2$ exchange with an automated chamber system throughout the year: Challenges in measuring night-time respiration on porous peat soil. *Biogeosciences* **2014**, *11*, 347–363. [CrossRef]
8. Liang, N.; Inoue, G.; Fujinuma, Y. A multichannel automated chamber system for continuous measurement of forest soil $CO_2$ efflux. *Tree Physiol.* **2003**, *23*, 825–832. [CrossRef] [PubMed]
9. McGinn, S.; Akinremi, O.; McLean, H.; Ellert, B. An automated chamber system for measuring soil respiration. *Can. J. Soil Sci.* **1998**, *78*, 573–579. [CrossRef]
10. Keeling, C.D. The concentration and isotopic abundances of atmospheric carbon dioxide in rural areas. *Geochim. Cosmochim. Acta* **1958**, *13*, 322–334. [CrossRef]
11. Zeeman, M.J.; Werner, R.A.; Eugster, W.; Siegwolf, R.T.W.; Wehrle, G.; Mohn, J.; Buchmann, N. Optimization of automated gas sample collection and isotope ratio mass spectrometric analysis of $\delta^{13}C$ of $CO_2$ in air. *Rapid Commun. Mass Spectrom.* **2008**, *22*, 3883–3892. [CrossRef]
12. Bowling, D.R.; Sargent, S.D.; Tanner, B.D.; Ehleringer, J.R. Tunable diode laser absorption spectroscopy for stable isotope studies of ecosystem–atmosphere $CO_2$ exchange. *Agric. For. Meteorol.* **2003**, *118*, 1–19. [CrossRef]
13. Guimbaud, C.; Noel, C.; Chartier, M.; Catoire, V.; Blessing, M.; Gourry, J.C.; Robert, C. A quantum cascade laser infrared spectrometer for $CO_2$ stable isotope analysis: Field implementation at a hydrocarbon contaminated site under bio-remediation. *J. Environ. Sci.* **2016**, *40*, 60–74. [CrossRef] [PubMed]
14. Nelson, D.D.; McManus, J.B.; Herndon, S.C.; Zahniser, M.S.; Tuzson, B.; Emmenegger, L. New method for isotopic ratio measurements of atmospheric carbon dioxide using a 4.3 μm pulsed quantum cascade laser. *Appl. Phys. B* **2008**, *90*, 301–309. [CrossRef]
15. Tuzson, B.; Zeeman, M.J.; Zahniser, M.S.; Emmenegger, L. Quantum cascade laser based spectrometer for in situ stable carbon dioxide isotope measurements. *Infrared Phys. Technol.* **2008**, *51*, 198–206. [CrossRef]
16. Wahl, E.H.; Fidric, B.; Rella, C.W.; Koulikov, S.; Tan, S.; Kachanov, A.A.; Richman, B.A.; Crosson, E.R.; Paldus, B.A.; Kalaskar, S.; et al. Applications of cavity ring-down spectroscopy to high precision isotope ratio measurement of $^{13}C/^{12}C$ in carbon dioxide. *Isotopes Environ. Health Stud.* **2006**, *42*, 20–35. [CrossRef] [PubMed]
17. McManus, J.B.; Nelson, D.D.; Shorter, J.H.; Jimenez, R.; Herndon, S.; Saleska, S.; Zahniser, M. A high precision pulsed quantum cascade laser spectrometer for measurements of stable isotopes of carbon dioxide. *J. Mod. Opt.* **2005**, *52*, 2309–2321. [CrossRef]
18. Sturm, P.; Eugster, W.; Knohl, A. Eddy covariance measurements of $CO_2$ isotopologues with a quantum cascade laser absorption spectrometer. *Agric. For. Meteorol.* **2012**, *152*, 73–82. [CrossRef]
19. Wehr, R.; Munger, J.W.; Nelson, D.D.; Mcmanus, J.B.; Zahniser, M.S.; Wofsy, S.C.; Saleska, S.R. Long-term eddy covariance measurements of the isotopic composition of the ecosystem–atmosphere exchange of $CO_2$ in a temperate forest. *Agric. For. Meteorol.* **2013**, *181*, 69–84. [CrossRef]
20. Gentsch, L.; Sturm, P.; Hammerle, A.; Siegwolf, R.; Wingate, L.; Ogée, J.; Baur, T.; Plüss, P.; Barthel, M.; Buchmann, N.; et al. Carbon isotope discrimination during branch photosynthesis of *Fagus sylvatica*: Field measurements using laser spectrometry. *J. Exp. Bot.* **2014**, *65*, 1481–1496. [CrossRef]
21. Kammer, A.; Tuzson, B.; Emmenegger, L.; Knohl, A.; Mohn, J.; Hagedorn, F. Application of a quantum cascade laser-based spectrometer in a closed chamber system for real-time $\delta^{13}C$ and $\delta^{18}O$ measurements of soil-respired $CO_2$. *Agric. For. Meteorol.* **2011**, *151*, 39–48. [CrossRef]
22. Guillon, S.; Pili, E.; Agrinier, P. Using a laser-based $CO_2$ carbon isotope analyser to investigate gas transfer in geological media. *Appl. Phys. B* **2012**, *107*, 449–457. [CrossRef]
23. Pitt, J.R.; Le Breton, M.; Allen, G.; Percival, C.J.; Gallagher, M.W.; Bauguitte, S.J.-B.; O'Shea, S.J.; Muller, J.B.A.; Zahniser, M.S.; Pyle, J.; et al. The development and evaluation of airborne in situ $N_2O$ and $CH_4$ sampling using a quantum cascade laser absorption spectrometer (QCLAS). *Atmos. Meas. Tech.* **2016**, *9*, 63–77. [CrossRef]
24. Wen, X.F.; Meng, Y.; Zhang, X.Y.; Sun, X.M.; Lee, X. Evaluating calibration strategies for isotope ratio infrared spectroscopy for atmospheric $^{13}CO_2/^{12}CO_2$ measurement. *Atmos. Meas. Tech.* **2013**, *6*, 1491–1501. [CrossRef]
25. Griffith, D.W.T. Calibration of isotopologue-specific optical trace gas analysers: A practical guide. *Atmos. Meas. Tech.* **2018**, *11*, 6189–6201. [CrossRef]

26. Sturm, P.; Tuzson, B.; Henne, S.; Emmenegger, L. Tracking isotopic signatures of $CO_2$ at the high altitude site Jungfraujoch with laser spectroscopy: Analytical improvements and representative results. *Atmos. Meas. Tech.* **2013**, *6*, 1659–1671. [CrossRef]
27. Pilegaard, K.; Hummelshøj, P.; Jensen, N.O.; Chen, Z. Two years of continuous $CO_2$ eddy-flux measurements over a Danish beech forest. *Agric. For. Meteorol.* **2001**, *107*, 29–41. [CrossRef]
28. Pilegaard, K.; Ibrom, A.; Courtney, M.S.; Hummelshøj, P.; Jensen, N.O. Increasing net $CO_2$ uptake by a Danish beech forest during the period from 1996 to 2009. *Agric. For. Meteorol.* **2011**, *151*, 934–946. [CrossRef]
29. Brændholt, A.; Larsen, K.S.; Ibrom, A.; Pilegaard, K. Partitioning of ecosystem respiration in a beech forest. *Agric. For. Meteorol.* **2018**, *252*, 88–98. [CrossRef]
30. LI-COR Biosciences. Capturing and Processing Soil GHG Fluxes Using the LI-8100A. 2014. Available online: https://www.licor.com/env/pdf/soil_flux/8100A_AppNote_GHG_Fluxes_15121.pdf (accessed on 15 April 2019).
31. Rothman, L.S.; Gordon, I.E.; Babikov, Y.; Barbe, A.; Benner, D.C.; Bernath, P.F.; Birk, M.; Bizzocchi, L.; Boudon, V.; Brown, L.R.; et al. The HITRAN2012 molecular spectroscopic database. *J. Quant. Spectrosc. Radiat. Transf.* **2013**, *130*, 4–50. [CrossRef]
32. R Core Team. *R: A Language and Environment for Statistical Computing*; R Foundation for Statistical Computing: Vienna, Austria, 2014.
33. Brændholt, A.; Larsen, K.S.; Ibrom, A.; Pilegaard, K. Overestimation of closed-chamber soil $CO_2$ effluxes at low atmospheric turbulence. *Biogeosciences* **2017**, *14*, 1603–1616. [CrossRef]
34. Braden-Behrens, J.; Yan, Y.; Knohl, A. A new instrument for stable isotope measurements of $^{13}C$ and $^{18}O$ in $CO_2$–instrument performance and ecological application of the Delta Ray IRIS analyzer. *Atmos. Meas. Tech.* **2017**, *10*, 4537–4560. [CrossRef]
35. Pang, J.; Wen, X.; Sun, X.; Huang, K. Intercomparison of two cavity ring-down spectroscopy analyzers for atmospheric $^{13}CO_2/^{12}CO_2$ measurement. *Atmos. Meas. Tech.* **2016**, *9*, 3879–3891. [CrossRef]
36. Vogel, F.R.; Huang, L.; Ernst, D.; Giroux, L.; Racki, S.; Worthy, D.E.J. Evaluation of a cavity ring-down spectrometer for in situ observations of $^{13}CO_2$. *Atmos. Meas. Tech.* **2013**, *6*, 301–308. [CrossRef]
37. McManus, J.B.; Nelson, D.D.; Zahniser, M.S. Design and performance of a dual-laser instrument for multiple isotopologues of carbon dioxide and water. *Opt. Express.* **2015**, *23*, 6518–6569. [CrossRef]
38. Formánek, P.; Ambus, P. Assessing the use of $\delta^{13}C$ natural abundance in separation of root and microbial respiration in a Danish beech (*Fagus sylvatica* L.) forest. *Rapid Commun. Mass Spectrom.* **2004**, *18*, 897–902. [CrossRef]
39. Wu, J.; Larsen, K.S.; van der Linden, L.; Beier, C.; Pilegaard, K.; Ibrom, A. Synthesis on the carbon budget and cycling in a Danish, temperate deciduous forest. *Agric. For. Meteorol.* **2013**, *181*, 94–107. [CrossRef]
40. Millard, P.; Midwood, A.J.; Hunt, J.E.; Barbour, M.M.; Whitehead, D. Quantifying the contribution of soil organic matter turnover to forest soil respiration, using natural abundance $\delta^{13}C$. *Soil Biol. Biochem.* **2010**, *42*, 935–943. [CrossRef]
41. Sakata, T.; Ishizuka, S.; Takahashi, M. Separation of soil respiration into $CO_2$ emission sources using $^{13}C$ natural abundance in a deciduous broad-leaved forest in Japan. *Soil Sci. Plant Nutr.* **2007**, *53*, 328–336. [CrossRef]
42. Andersen, C.P.; Nikolov, I.; Nikolova, P.; Matyssek, R.; Häberle, K.H. Estimating "autotrophic" belowground respiration in spruce and beech forests: Decreases following girdling. *Eur. J. For. Res.* **2005**, *124*, 155–163. [CrossRef]
43. Brumme, R. Mechanisms of carbon and nutrient release and retention in beech forest gaps. *Plant Soil* **1995**, *168*, 593–600. [CrossRef]
44. Epron, D.; Le Dantec, V.; Dufrene, E.; Granier, A. Seasonal dynamics of soil carbon dioxide efflux and simulated rhizosphere respiration in a beech forest. *Tree Physiol.* **2001**, *21*, 145–152. [CrossRef]
45. Epron, D.; Farque, L.; Lucot, E.; Badot, P.-M. Soil $CO_2$ efflux in a Beech Forest: The Contribution of Root Respiration. *Ann. For. Sci.* **1999**, *56*, 289–295. [CrossRef]
46. Silver, W.L.; Thompson, A.W.; McGroddy, M.E.; Varner, R.K.; Dias, J.D.; Silva, H.; Crill, P.M.; Keller, M. Fine root dynamics and trace gas fluxes in two lowland tropical forest soils. *Glob. Chang. Biol.* **2005**, *11*, 290–306. [CrossRef]
47. Subke, J.A.; Inglima, I.; Cotrufo, M.F. Trends and methodological impacts in soil $CO_2$ efflux partitioning: A metaanalytical review. *Glob. Chang. Biol.* **2006**, *12*, 921–943. [CrossRef]

48. Salomón, R.; Valbuena-Carabana, M.; Rodriguez-Calcerrada, J.; Aubrey, D.; McGuire, M.A.; Teskey, R.; Gil, L.; Gonzalez-Doncel, I. Xylem and soil $CO_2$ fluxes in a *Quercus pyrenaica* Willd. coppice: Root respiration increases with clonal size. *Ann. For. Sci.* **2015**, *72*, 1065–1078. [CrossRef]
49. Bekele, A.; Kellman, L.; Beltrami, H. Soil Profile $CO_2$ concentrations in forested and clear cut sites in Nova Scotia, Canada. *For. Ecol. Manag.* **2007**, *242*, 587–597. [CrossRef]
50. Kindler, R.; Siemens, J.; Kaiser, K.; Walmsley, D.C.; Bernhofer, C.; Buchmann, N.; Cellier, P.; Eugster, W.; Gleixner, G.; Grunwald, T.; et al. Dissolved carbon leaching from soil is a crucial component of the net ecosystem carbon balance. *Glob. Chang. Biol.* **2011**, *17*, 1167–1185. [CrossRef]
51. Yavitt, J.B.; Fahey, T.J.; Simmons, J.A. Methane and carbon-dioxide dynamics in a northern hardwood ecosystem. *Soil Sci. Soc. Am. J.* **1995**, *59*, 796–804. [CrossRef]
52. Nickerson, N.; Risk, D. Keeling plots are non-linear in non-steady state diffusive environments. *Geophys. Res. Lett.* **2009**, *36*, 6–9. [CrossRef]
53. Pataki, D.E.; Ehleringer, J.R.; Flanagan, L.B.; Yakir, D.; Bowling, D.R.; Still, C.J.; Buchmann, N.; Kaplan, J.O.; Berry, J.A. The Application and Interpretation of Keeling Plots in Terrestrial Carbon Cycle Research. *Glob. Biogeochem. Cycles* **2003**, *17*, 1022. [CrossRef]
54. Albanito, F.; Mcallister, J.L.; Cescatti, A.; Smith, P.; Robinson, D. Dual-chamber measurements of $\delta^{13}C$ of soil-respired $CO_2$ partitioned using a field-based three end-member model. *Soil Biol. Biochem.* **2012**, *47*, 106–115. [CrossRef]
55. Boone, R.D.; Nadelhoffer, K.J.; Canary, J.D.; Kaye, J.P. Roots exert a strong influence on the temperature sensitivity of soil respiration. *Nature* **1998**, *396*, 570–572. [CrossRef]
56. Graham, S.L.; Millard, P.; Hunt, J.E.; Rogers, G.N.D.; Whitehead, D. Roots affect the response of heterotrophic soil respiration to temperature in tussock grass microcosms. *Ann. Bot.* **2012**, *110*, 253–258. [CrossRef]
57. Schnyder, H.; Schäufele, R.; Lötscher, M.; Gebbing, T. Disentangling $CO_2$ fluxes: Direct measurements of mesocosm-scale natural abundance $^{13}CO_2/^{12}CO_2$ gas exchange, $^{13}C$ discrimination and labelling of $CO_2$ exchange flux components in controlled environments. *Plant Cell Environ.* **2003**, *26*, 1863–1874. [CrossRef]
58. Sun, W.; Resco, V.; Williams, D.G. Environmental and physiological controls on the carbon isotope composition of $CO_2$ respired by leaves and roots of a C3 woody legume (*Prosopis velutina*) and a C4 perennial grass (*Sporobolus wrightii*). *Plant Cell Environ.* **2012**, *35*, 567–577. [CrossRef]
59. Maunoury, F.; Berveiller, D.; Lelarge, C.; Pontailler, J.Y.; Vanbostal, L.; Damesin, C. Seasonal, daily and diurnal variations in the stable carbon isotope composition of carbon dioxide respired by tree trunks in a deciduous oak forest. *Oecologia* **2007**, *151*, 268–279. [CrossRef]
60. Teskey, R.O.; Mcguire, M.A. Measurement of stem respiration of sycamore (*Platanus occidentalis* L.) trees involves internal and external fluxes of $CO_2$ and possible transport of $CO_2$ from roots. *Plant Cell Environ.* **2007**, *30*, 570–579. [CrossRef] [PubMed]